

*Final
11-89
OCT*

**Final Report
NAG 5 2520**

“ASCA Observations of the Unusual Binary LSI+61° 303”

This NASA grant was provided to support ASCA observations of the unusual binary system LSI + 61°303. The observations were successfully carried out in January and February 1994. The grant supported the acquisition of a workstation for data analysis and travel to Calgary, CA to collaborate on the data analysis.

Analysis of the data have been completed and the results written up and submitted for publication to the Astrophysical Journal. The analysis was performed on the SUN Microsystems LX computer purchased for this purpose using software obtained from the NASA HEASARC. Dr. Fiona Harrison spent one week in Calgary to collaborate on the scientific interpretation. Preprints of the submitted papers are included as a summary of the scientific results.

Simultaneous X-ray and Radio Observations of the Unusual Binary LSI+61°303

Fiona A. Harrison¹

Space Radiation Laboratory, California Institute of Technology, Pasadena, CA 91125

Denis A. Leahy²

Department of Physics, University of Calgary, Calgary, Canada T2N 1N4

and

Elizabeth Waltman³

Remote Sensing Division, Naval Research Laboratory, Washington, DC 20375

ABSTRACT

We present simultaneous 0.5 – 10 keV X-ray and two-frequency radio observations at 2.25 and 8.3 GHz of the unusual binary system LSI +61°303 . This system was observed twice in a single binary orbit by the *ASCA* satellite, and monitored daily at two radio frequencies during the same orbital cycle with the Greenbank Interferometer. During the first *ASCA* observation the source was detected with a 1 – 10 keV luminosity $3.6 \times 10^{33} (d/2.0 \text{ kpc})^2 \text{ erg s}^{-1}$ and during the second at a similar level with evidence for a decrease in average flux of 30%. During the first pointing the radio source was at a quiescent 8 GHz flux level of 30 mJy while during the second the radio flux was rising dramatically with an average value of 100 mJy. No variability is seen in the X-ray flux during the first pointing, but during the second the flux is variable by $\sim 50\%$ on timescales of ~ 30 minutes. No pulsations are seen in either X-ray observation with an upper limit on pulsed flux of 20% . The low X-ray luminosity and lack of observed pulsations indicate that accretion onto a neutron star surface is not the origin for the high-energy emission. Rather, the X-rays must result either from accreted matter which is stopped at the magnetosphere because the magnetospheric boundary is rotating at super-Keplerian rates or due to a shock formed in the interaction of

¹E-mail: fiona@srl.caltech.edu

²E-mail: leahy@iras.ucalgary.ca

³E-mail: ewaltman@rira.nrl.navy.mil

the dense wind of the Be star companion and a moderately young pulsar. We derive a required pulsar spin down luminosity of $\sim 10^{37}$ erg s $^{-1}$, and argue that the shock model more easily explains the observed X-ray and radio observations.

Subject headings: stars: neutron – stars: individual: LSI +61°303 – binaries: radio – stars: emission line, Be – X-rays: stars

1 INTRODUCTION

The Be star LSI +61°303 is the optical counterpart of the periodic radio source GT 0236+610. The radio source is highly variable, exhibiting outbursts every 26.5 days which have rise times of ~ 1 day and last ~ 10 days (Gregory & Taylor 1978, Taylor & Gregory 1982). Two-frequency radio monitoring indicates a flat spectral index, and the emission has been interpreted as optically-thin synchrotron radiation for most of the outburst, with indication that the source becomes self-absorbed for a short time at the beginning of the outburst rise (Taylor & Gregory 1984). VLBI observations show that at its maximum size the emitting region has a dimension of $\sim 5 \times 10^{13}$ cm, and an expansion velocity $(2.0 - 6.4) \times 10^7$ cm s $^{-1}$ (Taylor *et al.* 1992a, Massi *et al.* 1993). The phase of peak flux varies between 0.4 – 1.0 of the radio ephemeris (phase 0 arbitrarily defined as MJD 43366.275), most often occurring at phase ~ 0.6 (Paredes, Estalella & Rius 1990, Ray *et al.* 1996). It has been suggested that the peak outburst flux is modulated on a four-year timescale (Gregory *et al.* 1989). Although it is evident that the peak radio flux is highly variable on timescales of several years, the four-year periodicity is not well established (Ray *et al.* 1996). Distance determinations place LSI +61°303 at 1.8 – 2.3 kpc (Gregory *et al.* 1979, Frail & Hjellming 1991).

Optical data show that the primary is a rapidly-rotating star of spectral type B0 V (Hutchings & Crampton 1981) or B0-B0.5 III (Paredes & Figueras 1986). Spectroscopic radial velocity measurements in the optical and UV confirm the binary nature of the system, and find an orbital period in agreement with that of the radio outbursts (Hutchings & Crampton 1981). The optical spectroscopic measurements of the system are however complicated by the composite and variable nature of the line emission (Hutchings & Crampton 1981), and have not yielded a good orbital solution. The best fit to these data imply a high-eccentricity of 0.6 – 0.8 and a periastron passage at radio phase of $\phi_p \sim 0.2$, although lower eccentricity fits are also possible. Orbital solutions derived from infrared photometric observations also imply high eccentricities (0.7 – 0.8), with a best-fit periastron passage at $\phi_p = 0.5$ (Marti & Paredes 1995). For this orbit and a Be star mass of $10 M_\odot$ the semimajor axis of the orbit is $4 - 6 \times 10^{12}$ cm. Infrared measurements imply the presence of a dense equatorial disk, and a mass-loss rate in the wind of $1 - 4 \times 10^{-7} M_\odot \text{ yr}^{-1}$ has been estimated from these observations assuming an opening angle of 15° for the disk and an initial wind velocity of 5 km s $^{-1}$ (Waters *et al.* 1988).

Originally detected by *Einstein*, LSI +61°303 is a weak X-ray source, with $L_x \sim 10^{33}$ ergs s $^{-1}$ (Bignami *et al.* 1981). *ROSAT* observations determined that the X-ray source is variable and has a harder spectrum than that characteristic of O and B stars (Goldoni & Mereghetti 1995). *ASCA* observations, presented here and in a companion paper, Leahy,

Harrison and Yoshida (1996) (hereafter LHY96), show that the spectrum is described by a relatively hard power-law, and therefore the emission mechanism is non-thermal in nature.

LSI +61°303 is particularly interesting due to the fact that it is located within the error box of the strong 100 MeV COS B source 2CG 135+01 (Bignami & Hermsen 1983). Recent EGRET observations have narrowed the error region, and currently LSI +61°303 is the most probable X-ray counterpart (von Montigny *et al.* 1993). COMPTEL has also detected emission in the 1 – 10 MeV band from the same region (van Dijk *et al.* 1994). No significant variability has been detected in the high-energy data, however the observation periods are typically two weeks and thus sample a large fraction of the binary orbit.

In this paper, we report on 0.5 – 10 keV X-ray observations with the *ASCA* satellite and simultaneous two-frequency (2 and 8 GHz) radio monitoring of LSI +61°303 using the Greenbank Interferometer (GBI). We present the simultaneous radio data, X-ray light-curve and X-ray timing analysis. Spectral analysis of the *ASCA* data is presented in a companion paper, LHY96.

2 OBSERVATIONS

In order to study the time-variability of the X-ray emission with orbital phase and search for possible correlations with radio intensity LSI +61°303 was observed twice during the same orbit by the *ASCA* satellite. The *ASCA* satellite carries on board four grazing-incidence X-ray telescopes sensitive in the energy range 0.5 – 10 keV. The focal plane of two telescopes contain gas imaging scintillation detectors (referred to as the GIS), and two contain silicon CCD detectors, (referred to as the SIS). The energy resolution of the GIS detectors is 8% at 5.9 keV, while that of the SIS detectors is considerably better; 2% at 5.9 keV. The temporal resolution of the GIS is better than the SIS, which for this observation was read out every 4 seconds, by a factor dependent on the telemetry and instrument modes.

The first pointing (hereafter referred to as P1) took place on 3 February 1994 (MJD 49386) beginning at 1:45 UT and ending at 11:01 UT, corresponding to phase 0.2 of the arbitrary radio ephemeris. The second observation (P2) began on 9 February 1994 (MJD 49392) at 7:34 UT and ended on the same day at 17:08 UT, corresponding to phase 0.43. Each observation yielded between 18,000 and 20,000 seconds of exposure time. The first observation was taken with the SIS in 2-CCD mode and a GIS temporal resolution of .0625 s. The second observation was taken in 1-CCD mode and a GIS temporal resolution of 0.5 s.

Throughout the entire binary orbit coincident with the *ASCA* pointings, we monitored the source frequently using the two-element Greenbank Interferometer (GBI). The

GBI consists of two 26 meter antennas each of which has a pair of cooled receivers which simultaneously receive signals at 2.25 and 8.3 GHz with a system bandwidth of 35 MHz. During the quiescent radio state LSI +61°303 was monitored every two days, and during the radio outburst the source was monitored 2 – 4 times every day. Each observation consists of a ten minute scan. Measured correlator amplitudes are converted to fluxes by comparing to standard, regularly observed calibrators. Constraints imposed by the radio telescope mount and elevation angle of the source precluded strict simultaneity of the X-ray and radio observations, however radio observations were performed closely prior to and following the *ASCA* pointings.

3 ANALYSIS AND RESULTS

Figure 1 shows the two-frequency radio data from the radio outburst coincident with the *ASCA* pointings. In general, the peak flux of the radio flare is quite variable outburst to outburst, and has been observed to occur anywhere in the phase range between 0.4 and 0.95. In the last 1.5 years, beginning with our simultaneous *ASCA* observations, LSI +61°303 has been monitored daily with the GBI, and the peak of the radio outburst has consistently fallen in the range 0.5 – 0.8 (Ray *et al.* 1996). The amplitude is also variable orbit to orbit, and some weak evidence has been presented that the amplitude variability is regularly modulated with a period of four years (Gregory *et al.* 1989).

For the outburst coincident with our *ASCA* observations the peak in the radio flux occurs at phase 0.5, with a maximum amplitude at 2 GHz of 190 mJy. As can be seen in Figure 1, P1 took place before the radio outburst, while P2 occurred during the rise of the radio emission. During the first *ASCA* observation on MJD 49386, the radio flux averaged over three ten-minute observations taken between UT 1:45 and 11:03 was 39 ± 5 (1 σ) mJy and 27 ± 4 mJy at 2 and 8 GHz respectively. Figure 2 shows the radio flux measurements taken near P2. It can be seen that the radio flux is rising in intensity prior to P2, and is observed to increase dramatically immediately afterwards. Due to constraints on the GBI pointing, the source could not be monitored during the entire *ASCA* observation, however the radio flux is likely increasing during this observation.

The radio spectral index, γ (where $F(\nu) \propto \nu^{-\gamma}$) for the orbit coincident with the *ASCA* observations is shown in Figure 3. During most of the orbit $\gamma \sim 0.25$, however at the beginning of the radio flux increase the spectrum flattens to $\gamma \sim -0.1$. This is likely due to self-absorption in the synchrotron source.

The *ASCA* spectral data were analyzed using standardized analysis tools as described in LHY96. The spectrum of LSI +61°303 is best described by a power law of photon spectral

index $\alpha \sim 1.7$ (where $dN/dE \propto E^{-\alpha}$), with column depth of $6.0 \pm 0.5 \times 10^{21} \text{ cm}^{-2}$ (90% confidence). Some evidence for variability is seen in the X-ray intensity between the two *ASCA* pointings. For P1, the .5 - 10 keV flux, derived from joint fits to data from all four telescopes, is $7.2 \pm 0.7 \times 10^{-12} \text{ erg cm}^{-2}\text{s}^{-1}\text{keV}^{-1}$, and for P2 is $5.2 \pm 0.5 \times 10^{-12} \text{ erg cm}^{-2}\text{s}^{-1}\text{keV}^{-1}$, where the errors are 90% confidence. Thus there is some indication of a decrease in average flux at about the 90% confidence level between P1 and P2, however the X-ray flux during P2 was found to be variable. The X-ray spectrum also appears to be softer during the second pointing, being described by a photon spectral index of 1.71 ± 0.08 for P1, and a value 1.83 ± 0.08 for P2 (90% confidence errors).

3.1 SEARCH FOR PULSATIONS

We performed a pulsation search on the *ASCA* data to look for a signature of the neutron star postulated to be the compact companion in this binary. For the GIS detectors during P1 the time resolution of .0625 s limits the search to a minimum period of 0.125 s, and for P2, the minimum period searched is 1.0 s, corresponding to the Nyquist limit for the 0.5 s sampling. Epoch folding using the standard XRONOS software failed to detect periodicity in either pointing. The 90% confidence upper limits on the amplitude of pulsed emission are summarized in Table 1 for searches on the separate and combined GIS 1 and 2 data. These limits were calculated using the formalism described in Leahy *et al.* (1983). A second source in the FOV, identified as a stellar source (LHY96), labeled Source2, was also searched for pulsations, and the upper limits are also given in Table 5. For P1, in addition to the epoch folding an FFT was also performed, which yielded nearly identical upper limits on the pulsed amplitude fraction as the epoch folding. For P2, aperiodic variability in the source precluded the use of an FFT for period searching (see § 3.2). The SIS data were also searched down to a minimum period of 8 s, (determined by the 4 s readout time), and no pulsations were found, with limits similar to those presented for the GIS.

It has been suggested that the system may contain a moderately young pulsar with period in the range .05 – .5 s (Maraschi & Treves 1981, Zamanov 1995). To search for short-period pulsations, for which smearing of the pulsed signal due to variable Doppler shifts resulting from the binary orbital motion can be important, we performed an acceleration search on the GIS data from P1. The high orbital eccentricity implied for LSI +61°303 indicates that during some parts of the orbit the orbital acceleration may be large. Using the orbital solutions of Hutchings & Crampton (1981) a pulsed signal of period $\lesssim 1$ s will become decoherent in the *ASCA* observation time for some parts of the orbit. The variation in the pulse frequency is well-approximated by a linear trend over the duration of each observation. We therefore searched a range of constant frequency derivatives from $-3.6 \times 10^{-7} \text{ s}^{-2} <$

$\dot{\nu} < 3.6 \times 10^{-7} \text{s}^{-2}$ (consistent with the range expected from the orbital solutions) in 1600 spacings. No periodicity was detected.

3.2 APERIODIC VARIABILITY

Aperiodic variability with characteristic timescales of ~ 30 minutes has been observed at radio wavelengths during outburst (Gregory *et al.* 1979). We searched for similar variability in the data from the two GIS detectors, and found that during P1 the flux is consistent with a constant value, however during P2 the X-ray emission is variable on similar timescales to those seen in the radio. Figure 4 shows lightcurves, binned in 5 minute intervals, from the two GIS detectors combined for the two pointings. The variability by more than 50% is evident in the second data set. The short gaps in the lightcurves are due to passage through the South Atlantic Anomaly and Earth occultations.

In order to search for smaller-amplitude variability during P1, and characterize the fastest time scales of the variability seen during P2 we used a Lomb normalized periodogram (Press *et al.* 1992 and references therein). This technique does not introduce features due to data gaps which would normally appear using standard Fourier analysis, as the data are evaluated only at times that they are actually measured. It is important in this case because data gaps due to SAA passage and earth occultation occur at ~ 90 minute intervals, and thus introduce spurious power at frequencies similar to that of the X-ray variability. A periodogram of the data from P1 indicates no power at any frequency up to the Nyquist frequency, and is entirely consistent with Poisson noise. Highly-significant power is seen in the data from P2 with the highest frequencies of 10^{-4}s^{-1} , indicating variability on timescales of ~ 40 minutes. This implies a limit on the characteristic size for the emission region of $\lesssim 6 \times 10^{13} \text{cm}$, or $\sim 4 \text{AU}$.

4 DISCUSSION

The lack of a secure orbital solution for the system and the unknown nature of the compact companion complicate the interpretation of the observations. If the companion is a neutron star, the mechanisms for producing the radio and high-energy emission are strongly dependent on the neutron star spin period, magnetic field and orbit. Several models have been suggested to explain the radio outbursts, and the X-ray and gamma-ray emission associated with LSI +61°303. We discuss these models and the constraints on the nature of the compact companion in light of the simultaneous *ASCA* and GBI data, adopting the eccentric orbit and dense Be star wind indicated by the optical and IR observations.

4.1 X-ray Emission from the Be Star

The low X-ray luminosity of LSI +61°303 compared to typical high-mass X-ray binaries suggests that the X-ray emission could be due to the radiation-driven stellar wind of the Be star. The bolometric luminosity of the star is $1.5 \times 10^{38} \text{ erg s}^{-1}$ (Gregory *et al.* 1979), yielding a ratio $(L_x/L_{bol}) \sim 3 \times 10^{-5}$. This is within the range of $10^{-8} - 10^{-4}$ found in a *ROSAT* survey of OB and OBe stars (Meurs *et al.* 1992). However, the non-thermal nature of the X-ray emission is not consistent with the thermal B star spectra ($kT < 1 \text{ keV}$) (Cassinelli *et al.* 1994), and therefore the Be star is an unlikely source for the X-ray emission.

4.2 Accretion onto a Neutron Star Surface

Taylor *et al.* (Taylor & Gregory 1982, Taylor *et al.* 1992b) suggest that the radio outbursts are produced by events of super-Eddington accretion onto a neutron star occurring at periastron passage. They postulate that these events would produce a relativistic plasma which subsequently expands, radiating synchrotron radio emission. Using the optically-derived orbit and Be star wind parameters suggested by the IR data, super-Eddington accretion rates are expected for a large fraction of the orbit for eccentricities greater than ~ 0.3 (Taylor *et al.* 1992b). The *ASCA* observations at phases 0.2 and 0.43 sample portions of the orbit where high accretion rates would be expected for any of the high-eccentricity orbital solutions suggested by the IR or the optical data (either $\phi_p = 0.2$ or 0.5). The expected X-ray luminosity is 4 – 5 orders of magnitude larger than observed. Even if the gamma-ray luminosity is associated with the system it is still underluminous by a factor of at least 100. The lack of either Fe line features in the spectrum (LHY96) or X-ray pulsations is also inconsistent with this scenario. The observations are therefore not consistent with accretion of a significant fraction of the captured material onto a neutron star surface.

4.3 Accretion onto a Neutron Star Magnetosphere

If the neutron star magnetosphere rotates at a super-Keplerian rate accretion onto the neutron star surface will be inhibited by centrifugal forces, the accreted matter is stopped at the magnetosphere, and an accretion luminosity of only

$$L_{acc} = \frac{GM_p \dot{M}}{r_m} \quad (1)$$

where r_m is the magnetospheric radius, will be released (Stella *et al.* 1994). The accreted matter may either accumulate, forming a quasi-steady atmosphere (Davies & Pringle 1981), or be flung off (“the propeller effect”) (Illarionov & Sunyaev 1975). This mechanism has been invoked to explain the low X-ray luminosity of LSI +61°303 (Campana *et al.* 1995, Zamanov 1995). If the orbit is eccentric ($\epsilon \gtrsim 0.6$) then the mass capture rates expected at periastron predict an accretion luminosity of $\sim 10^{35}$ erg s⁻¹ (Campana *et al.* 1995), in excess of the observed X-ray luminosity, but comparable to the total high-energy emission if the gamma-ray flux is associated with the system. In this case the high-energy emission could be generated for a neutron star with magnetic moment $\mu \sim 6 \times 10^{31}$ G cm³ and spin period $0.3 \text{ s} < P < 25 \text{ s}$ (Campana *et al.* 1995).

If the high-energy emission is produced by accretion onto a neutron star magnetosphere, then the radio outbursts could result from an increase in the accretion rate due to the orbital eccentricity, perhaps as the material is ejected from the system. In this case, however, an increase in the X-ray flux would be expected to coincide with the beginning of the radio outburst, and a large variation in X-ray luminosity between the two *ASCA* pointings would be expected. In addition the X-ray spectral index should change more dramatically than observed for large changes in mass accretion rate.

4.4 Shock Emission

Marashi and Treves (1981) suggested that the observed properties of LSI +61°303 could be explained by emission from a shock produced at the interaction front between the dense Be star wind and the relativistic wind of a moderately young pulsar. The same mechanism has been proposed to explain the X-ray emission from PSR B1259-63, a 47 ms radio pulsar/Be system in a 3.4 yr, highly eccentric orbit. LSI +61°303 and B1259-63 have similar X-ray properties: a 1 – 10 keV luminosity of $\sim 1 \times 10^{34} (d/2 \text{ kpc})^2$ erg s⁻¹ and a power law spectrum with photon index 1.5 – 1.9 was measured by *ASCA* for B1259-63 before and after periastron, with a flux a factor ~ 2 smaller at periastron (Kaspi *et al.* 1995). In addition continuum radio emission has been detected from B1259-63 which increases by almost an order of magnitude near periastron (Johnston 1996).

In order to form a shock outside the accretion radius, R_{acc} , the pressure due to the relativistic pulsar wind must exceed the ram pressure due to the Be star wind,

$$P_p(R_{acc}) > P_w(R_{acc}), \quad (2)$$

where $R_{acc} = 2GM_p/v_{rel}^2$, and v_{rel} is the relative velocity between the pulsar and the Be star

wind. The pulsar radiation pressure is given by,

$$P_p = \frac{f\dot{E}}{4\pi cR^2}. \quad (3)$$

Adopting the standard magnetic dipole model, the pulsar spin down energy, \dot{E} is given by

$$\dot{E} = 6 \times 10^{35} \frac{B_{12}^2 R_6^6}{T_{-1}^4} \text{ erg s}^{-1}, \quad (4)$$

where B_{12} is the magnetic field strength in units of 10^{12} gauss, R_6 is the neutron star radius in units of 10^6 cm, T_{-1} is the pulsar spin period in units of 0.1 s, and $f \sim 1$.

We have estimated the required pulsar luminosity using the disk model for Be star winds, the eccentric orbital solutions derived from the IR data, and assuming the pulsar orbits in the plane of the Be star wind. The Be wind density is described by a power law ($\rho_w \propto r^{-n}$), the wind velocity dependence is $v_w \propto r^{n-2}$ and we adopt the wind parameters $n = 3.2$, $\dot{M} = 2 \times 10^{-7} M_\odot$, and an initial velocity at the stellar surface of 5 km s^{-1} suggested by IR observations (Waters *et al.* 1988). The pulsar luminosity required in order to avoid accretion near periastron, where the Be wind density and relative velocity are maximum is $1 - 3 \times 10^{37} \text{ erg s}^{-1}$, implying a ratio of pulsar spin down energy to X-ray luminosity of $L_x/\dot{E} \sim .03\%$, significantly smaller than the 0.9% measured for B1259-63 (Kaspi *et al.* 1995). If the gamma-ray luminosity is associated with the shock emission, then the ratio of high-energy luminosity to spin down energy is $\sim 1\%$, comparable to B1259-63. For a neutron star of radius 10^6 cm and surface magnetic field of 10^{12} Gauss a dipole luminosity of $10^{37} \text{ erg s}^{-1}$ implies a rotation period of ~ 50 ms.

For LSI +61°303 the large change in radio emission simultaneous with a slight decrease in the X-ray luminosity could be explained in this scenario by a change in the magnetic field at the shock as the shock region moves closer to the pulsar near periastron. The ~ 30 minute variability reported here in the X-ray and previously observed in the radio during outburst (Gregory *et al.* 1979) indicates that a common electron population is producing the low and high-energy emission, although detection of correlated variability in strictly-simultaneous observations is required for this to be conclusive. In this case synchrotron processes would produce the radio emission, with inverse Compton scattering of optical photons from the Be star on the same electron population producing the X-ray emission. The high implied magnetic field of ~ 300 Gauss (LHY96) would place the shock close to the neutron star, just outside the accretion radius. The observed expansion of the radio source after outburst could be due to the expansion of the region dominated by the pulsar wind as the neutron star moves away from the Be star. It is not however clear what would cause the radio outburst peak to vary substantially in phase orbit to orbit.

Table 1

	P1		P2	
LSI +61°303	# events	Amplitude Limit	# events	Amplitude Limit
GIS 1	2638	0.28	2159	0.24
GIS 2	2629	0.28	2585	0.22
GIS 1 + 2	5267	0.20	4744	0.16
Source2				
GIS 1	455	0.68	690	0.42
GIS 2	434	0.70	738	0.40
GIS 1 + 2	889	0.49	1428	0.29

REFERENCES

- Bignami, G., Caraveo, P., Lamb, R., Markert, T., and Paul, J. 1981, *ApJ*, 247, L85.
- Bignami, G. and Hermsen, W. 1983, *Ann. Rev. A&A*, 21, 67.
- Campana, S., Stella, L., Mereghetti, S., and Colpi, M. 1995, *A&A*, 297, 385.
- Cassinelli, J., Cohen, D., MacFarlane, J., Sanders, W., and Welsh, B. 1994, *ApJ*, 421, 705.
- Davies, R. and Pringle, J. 1981, *MNRAS*, 196, 209.
- Frail, D. and Hjellming, R. 1991, *AJ*, 101, 2126.
- Goldoni, P. and Mereghetti, S. 1995, *A&A*, 299, 751.
- Gregory, P., Xu, H., Backhouse, C., and Reid, A. 1989, *ApJ*, 339, 1054.
- Gregory, P. *et al.* 1979, *AJ*, 84, 1030.
- Gregory, P. C. and Taylor, A. R. 1978, *Nature*, 272, 704.
- Hutchings, J. B. and Crampton, D. 1981, *Publ. Astr. Soc. Pacific*, 93, 486.
- Illarionov, A. and Sunyaev, R. 1975, *A&A*, 39, 185.
- Johnston, S. 1996, Presented at the Sydney pulsar conference.
- Kaspi, V. M., Tavani, M., Nagase, F., *et al.* 1995, *ApJ*, 453, 424.
- Leahy, D., Darbro, W., Elsner, R., Weisskopf, M., Sutherland, P., Kahn, S., and Grindlay, J. 1983, *ApJ*, 266, 160.
- Maraschi, L. and Treves, A. 1981, *MNRAS*, 194, 1P.
- Marti, J. and Paredes, J. 1995, *A&A*, 298, 151.
- Massi, M., Paredes, J., Estalella, R., and Felli, M. 1993, *A&A*, 269, 249.
- Meurs, E. J. A., Pijpers, A., Pols, O., Waters, L., *et al.* 1992, *A&A*, 265, L41.
- Paredes, J., Estalella, R., and Rius, A. 1990, *A&A*, 232, 377.
- Paredes, J. and Figueras, F. 1986, *A&A*, 154, L30.

- Press, W. A., Teukolsky, S. A., Vetterling, W. T., and Flannery, B. P. 1992. Numerical Recipes in C, 575. Cambridge University Press.
- Ray, P. S., Foster, R. S., Waltman, E. B., Ghigo, F. D., and Tavani, M. 1996, in preparation.
- Stella, L., Campana, S., Colpi, M., Mereghetti, S., and Tavani, M. 1994, *ApJ*, 423, L47.
- Taylor, A. and Gregory, P. 1984, *ApJ*, 283, 273.
- Taylor, A., Kenny, H., Spencer, R., and Tzioumis, A. 1992a, *ApJ*, 395, 268.
- Taylor, A. R. and Gregory, P. C. 1982, *ApJ*, 255, 210.
- Taylor, A. R., Kenny, H. T., Spencer, R. E., and Tzioumis, A. 1992b, *ApJ*, 395, 268.
- van Dijk, R., Bloemen, H., Hermsen, W., Collmar, W., Dihl, R., *et al.* 1994, in *The Evolution of X-ray Binaries*, (New York: AIP Press), 324.
- von Montigny, K. *et al.* 1993. IAU circular 5708.
- Waters, L., Taylor, A., van den Heuvel, E., Habets, M., and Persi, P. 1988, *A&A*, 198, 200.
- Zamanov, R. K. 1995, *MNRAS*, 272, 308.

FIGURE CAPTIONS

FIGURE 1: Two-frequency radio data from the monitoring of LSI +61°303 during the outburst coincident with the *ASCA* X-ray observations. Indicated on the plot are the times corresponding to the two *ASCA* pointings.

FIGURE 2: Expanded plot of two frequency radio data taken shortly before and after the second *ASCA* pointing. The flux is seen to be increasing before and after the X-ray data were taken.

FIGURE 3: Radio spectral index for the orbit-outburst cycle coincident with the *ASCA* pointings. Here the spectral index γ is defined as $F(\nu) \propto \nu^{-\gamma}$.

FIGURE 4: Countrate in the 1 – 5 keV band from LSI +61°303 for the two *ASCA* pointings. The first pointing is consistent with no variability on any timescale, whereas during the second pointing the source varies by $\sim 50\%$ on timescales of 30 minutes.

Figure 1

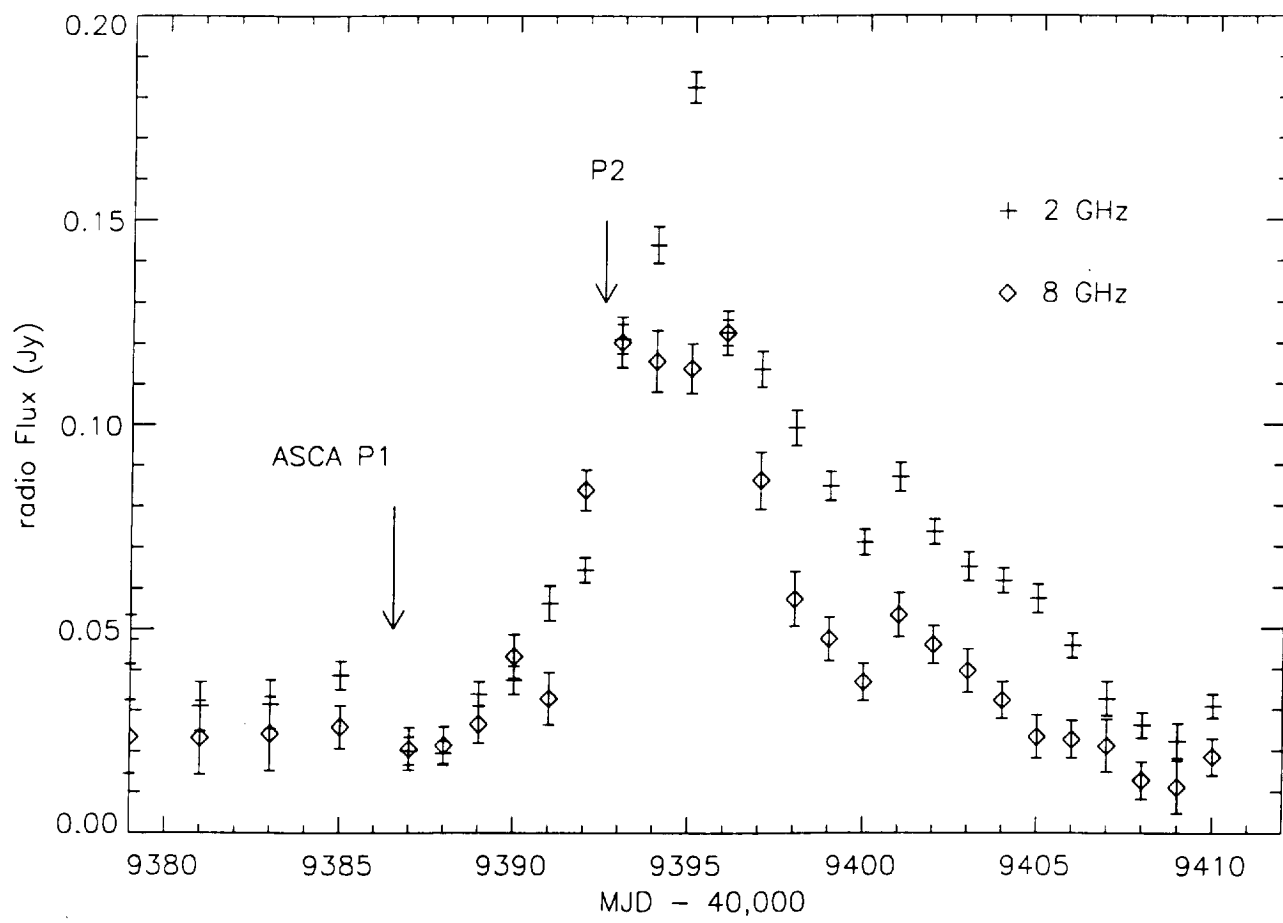


Figure 2

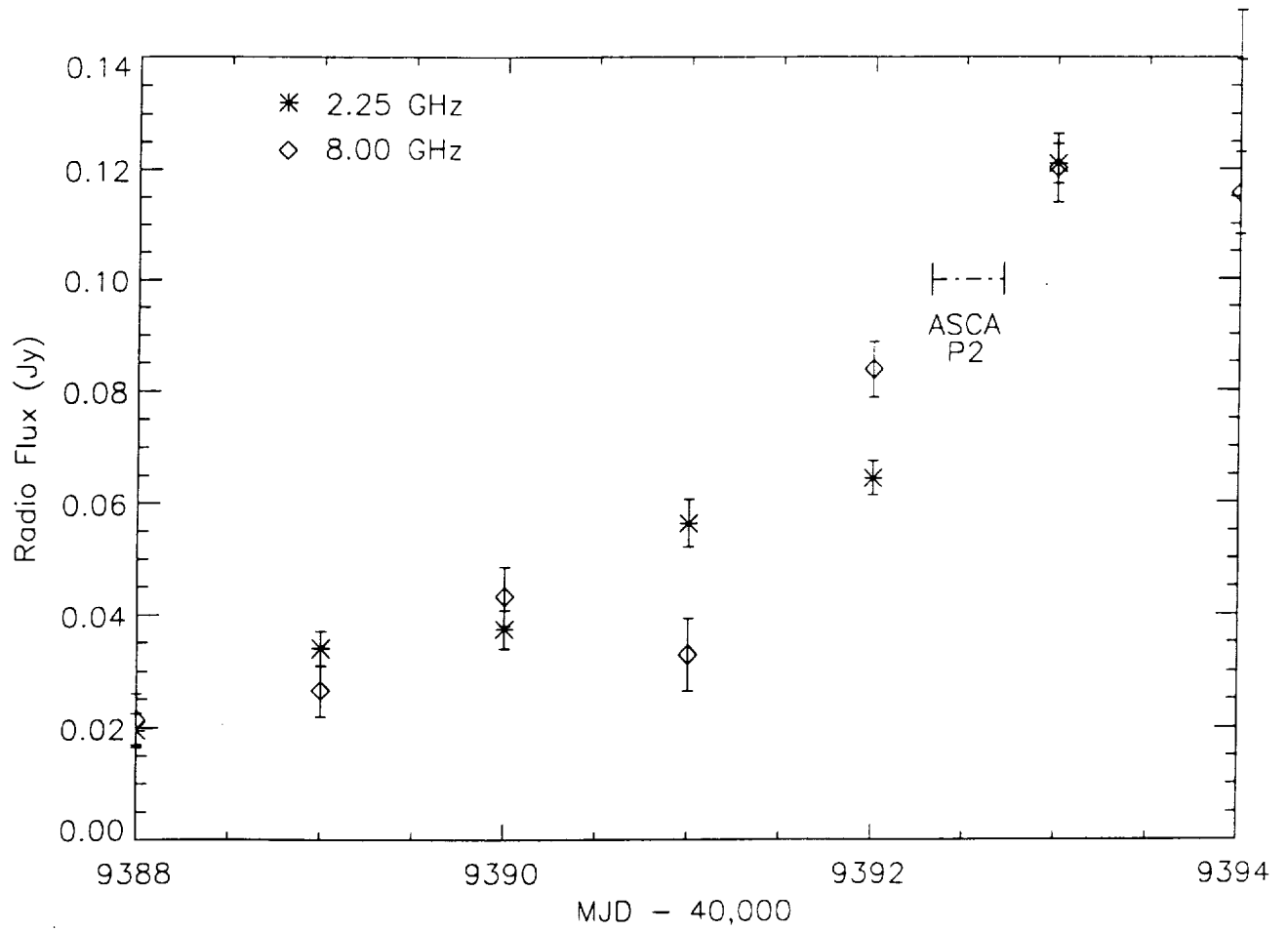


Figure 3

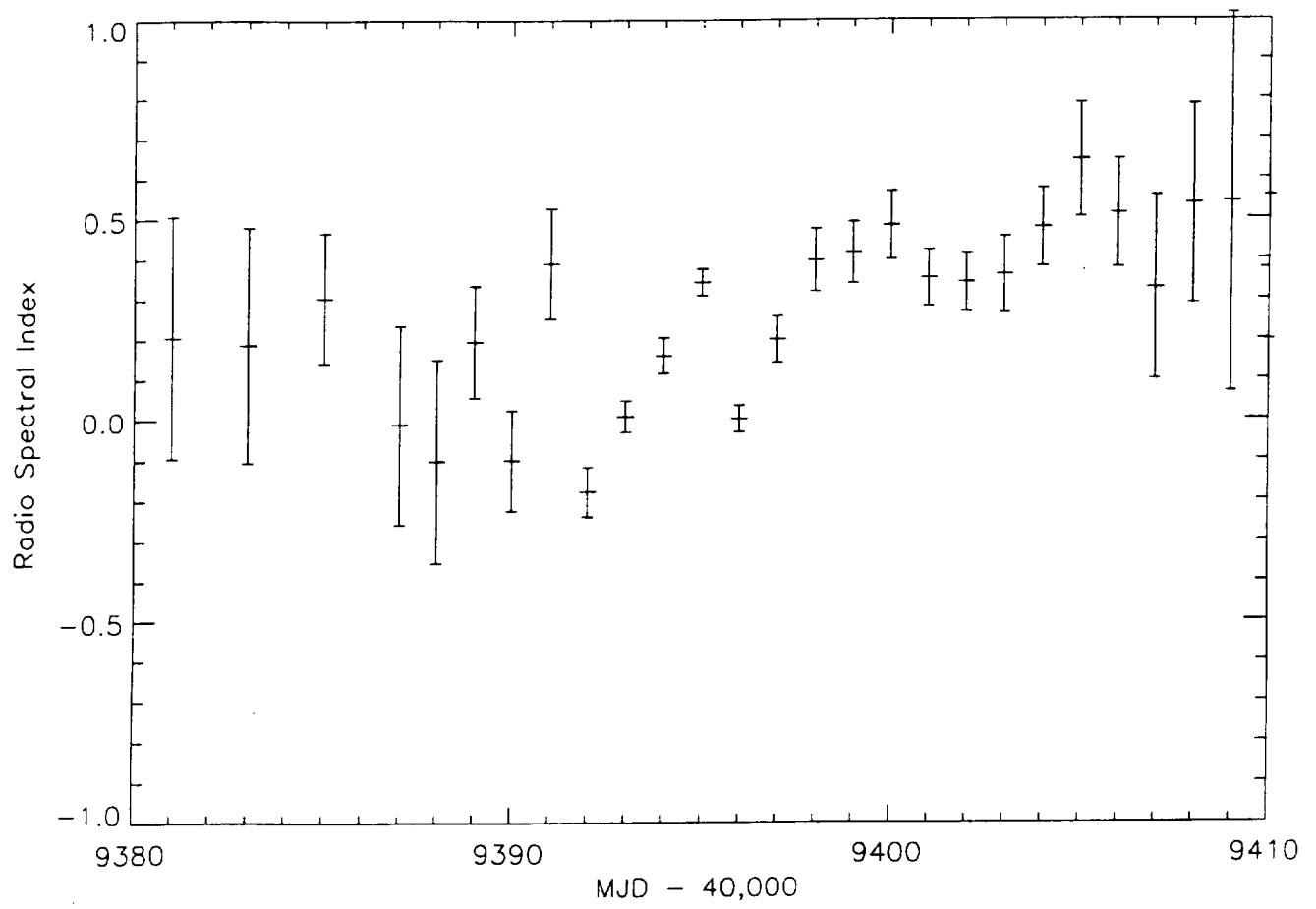
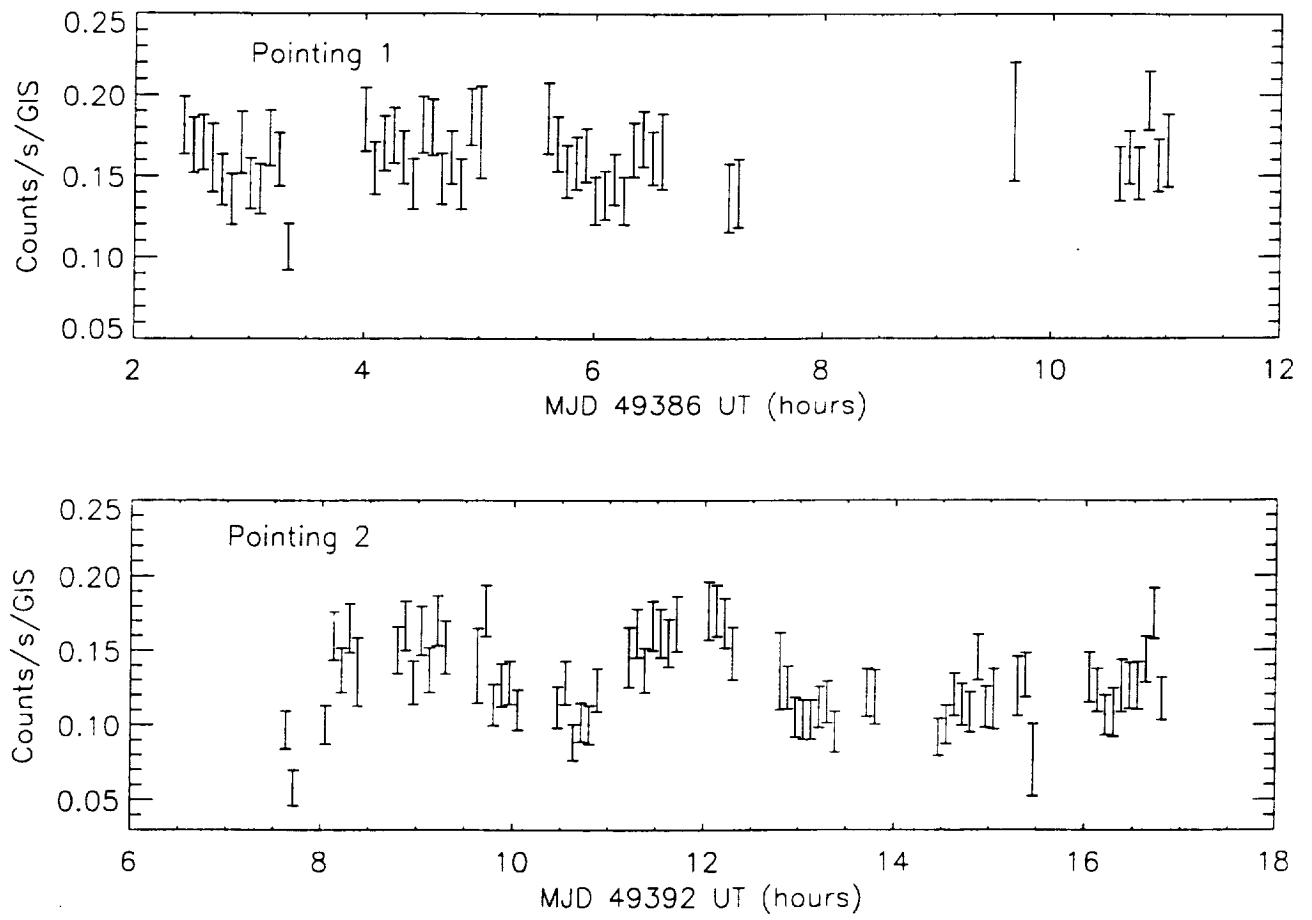


Figure 4



The ASCA X-ray Spectrum of the Unusual Binary LSI+61°303

Denis A. Leahy¹

Department of Physics, University of Calgary, Calgary, Canada T2N 1N4

Fiona A. Harrison²

Space Radiation Laboratory, California Institute of Technology, Pasadena, CA 91125

and

Atsumasa Yoshida³

Institute of Physical and Chemical Research, Saitama 351-01 Japan

ABSTRACT

The unusual Be binary LSI +61°303 was observed by the ASCA X-ray satellite twice during the 26 day orbital – outburst cycle. Here we present the results of the spectral analysis of the ASCA data. The emission spectrum can be characterized by an absorbed power law and is inconsistent with other single component models such as black body or hot plasma emission. The X-ray derived column density is the best determination so far for LSI +61°303 . The power law index is similar to that seen for classical X-ray pulsars, however the low X-ray luminosity and the power law emission in other wavebands indicate that the emission is not directly from an accretion column but rather synchrotron or inverse Compton emission from relativistic particles. We put a strong upper limit on Fe line emission. The data indicate both flux and spectral variability between the two observations.

Subject headings: stars: neutron – stars: individual: LSI +61°303 – binaries: radio – stars: emission line, Be – X-rays: stars

¹E-mail: leahy@iras.ucalgary.ca

²E-mail: fiona@citsrl.caltech.edu

³E-mail: ayoshida@postman.riken.go.jp

1 INTRODUCTION

LSI +61°303 is one of a small but important group of radio emitting X-ray binary systems. Well known members of this class include SS 433, CygX-1, CygX-3 and Circinus X-1. Considerable interest has centered around LSI +61°303 since 1977 when it was discovered to be strong, variable radio source (Gregory and Taylor 1978) and proposed to be the counterpart of the COS-B gamma-ray source 2CG 135+01. It was soon identified with its optical counterpart (Gregory et al. 1979). The radio light curve exhibits outbursts whose periodicity corresponds to the optical periodicity of the orbital motion (Hutchings and Crampton 1981).

LSI 61 303 has been also identified as an X-ray (Bignami et al. 1981) and possibly an MeV gamma-ray source ((van Dijk et al. 1993)). It was possibly detected in high energy (500 keV – 1 MeV) X-rays (Perotti et al. 1980), however these results are inconsistent with other spectral information (see discussion in Section 4.1 below).

Here we present the results of the analysis of the ASCA images and X-ray spectra of LSI 61 303. Analysis of the time variability and simultaneous radio observations of LSI 61 303 are presented in a following paper (Harrison et al. 1996).

2 OBSERVATIONS

LSI +61°303 was observed by ASCA (Tanaka et al. 1994) during two portions of the same 26 day cycle. ASCA has four identical thin foil light-weight X-ray telescopes which focus X-rays onto one of two Solid state Imaging Spectrometers (SIS) or one of two Gas Imaging Spectrometers (GIS). Hereafter the two SIS are referred to as S0 and S1, the two GIS as S2 and S3.

The first pointing took place on Feb 3, 1994 (MJD 49386) starting at 1:45 UT and ending at 11:01 UT, corresponding to radio phase 0.2. The second pointing took place on Feb 9, 1994 (MJD 49392) starting at 7:34 UT and ending at 17:08 UT, corresponding to radio phase 0.43. Binary radio phase was calculated using the 26.496 day arbitrary ephemeris of Taylor *et al.* (1984). The first pointing will be referred to as P1 hereafter, the second pointing as P2. For P1, the S0 and S1 net exposure times were 18843 and 18803 s, the S2 and S3 exposure times were both 17961 s. For P2, the S0 and S1 times were 33645 and 33639 s, the S2 and S3 times were 19344 and 19347 s.

All of the CCD (S0 and S1) observations were taken in faint mode (2-CCD mode for the first pointing and 1-CCD mode for the second). The absorbing column is constant between

the two observations. The data processing was carried out at The Institute of Physical and Chemical Research, Tokyo, using the ASCA reduction software, and a standardized set of reduction methods. This included filtering the data to remove hot pixels from the CCD data and observation intervals with high background (i.e. telescope pointings close to the earth's limb or after SAA passage).

3 ANALYSIS AND RESULTS

3.1 X-ray Image

The S2 image for the second pointing (P2) is shown in Fig. 1 in contour map form, labelled with 1950 coordinates. LSI +61°303 is the bright source near the center. The position is consistent with the published position of RA 40.115 degrees, Dec. +61.235 (J2000) (Gregory et al. 1979).

There is a second point source 7' southwest of LSI +61°303 . This source is seen in the same location in all of the GIS images (both detectors, both pointings). It is not seen in the SIS images, as it is just outside of the SIS field of view. Hereafter this source is referred to as Source 2. The position of Source 2 corresponds to RA 39.976 degrees, Dec. +61.128 (J2000), with an accuracy of 0.004 degrees.

3.2 Spectrum Analysis

For LSI +61°303 spectra were extracted from the event files for both pointings. For the SIS detectors, the source and background regions were taken approximately 3.2' in radius. For the GIS detectors the regions were 4.9' in radius. For Source 2, seen only in the GIS detectors, the source region was 3.4' in radius. The background subtracted count rates for the two pointings and the two sources (LSI +61°303 and Source 2) are given in Table 1. This shows that both sources are highly significant detections.

The resulting S0 and S1 spectra were rebinned from 4096 to 512 spectral channels. Then all (SIS and GIS) spectra were further rebinned to have minimum 20 counts per bin, so that a χ^2 statistic for fitting is applicable. The highest channels, which were consistent with zero counts, were ignored in the spectral fits. This resulted in spectra with about 120 channels with 20 or more counts for LSI +61°303 , and with about 40 channels with 20 or more counts for Source 2.

Spectral fits were made using power law, Raymond-Smith and blackbody models. For all models parameter 1 (hereafter Param1) was column density, and Param3 is the normalization. For the blackbody and Raymond-Smith models Param2 is temperature in keV units; for the power law model, Param2 is the power-law index. The power law model is referred to as 'power', the Raymond-Smith model as 'raym', and the blackbody model as 'bbdy'. χ_r^2 is the reduced χ^2 value of the fit. Table 2 lists the results of the spectral fits to the eight SIS and GIS individual spectra of LSI +61°303. Table 3 shows the results for fits to the four GIS spectra of Source 2 (discussed below).

3.3 ASCA Spectra of LSI +61°303

The observed spectrum for LSI +61°303 from the S0 detector for P1, and the best fit power law model spectra is shown in Figure 2. Figure 3 shows the S2, P1 spectrum and best fit power law model. These power law fits are statistically acceptable (see Table 2), as are the fits using the Raymond-Smith model. However the blackbody fits are significantly worse, and are rejected on this basis and also because the implied column density is unacceptably low. The Raymond-Smith model gives slightly higher χ_r^2 values than the power law, and also gives significantly lower column densities and high temperatures (of order 10 to 20 keV).

The four spectra for each pointing (S0, S1, S2 and S3) were fit simultaneously with a single model (referred to as joint fits). Table 4 shows the results of joint fits for both LSI +61°303 and Source 2 (Source 2 only has S2 and S3 spectra and is discussed below). Again the blackbody had higher χ_r^2 and unacceptably low column density, so can be rejected. The Raymond-Smith spectra have higher χ_r^2 and lower column density than the power law fits, and again show high temperatures. The power law model is preferred on the basis of χ_r^2 alone, but considering the column density of 10^{22}cm^{-2} to LSI +61°303 measured in radio (Frail and Hjellming 1991), it is the only acceptable spectral model.

The derived column densities for the two observations, P1 and P2 agree. The 2-10 keV flux is 30% lower for P2 than P1, and the 0.5-2 keV flux is 17% lower. The data also indicate a difference in power law index (or temperature, for the Raymond-Smith model), at about the 90% confidence level: the P2 spectrum is softer (or cooler). Joint fits to all of the ASCA spectra from both pointings were done. The χ_r^2 values were significantly higher than for fits to data from the individual pointings. This can be attributed to the different power law index (or temperature) between the pointings. The parameters for the joint fits to both pointings were intermediate between those for P1 and P2, as expected. The blackbody fit was rejected even more strongly.

The observed spectra of LSI +61°303 show no discernable iron emission line at 6.4 keV, nor any iron absorption edge (see Figs. 2 and 3). From fits which include a 6.4 keV (0.1 keV width) iron emission line in the model, 3 sigma upper limits for the iron line intensity of 1.4×10^{-5} ph cm⁻² s⁻¹ (power law spectrum) or 4.5×10^{-6} ph cm⁻² s⁻¹ (Raymond-Smith spectrum) are derived. Similarly, the 3 sigma upper limits on optical depth of a 7.1 keV iron edge were found to be 0.51 (power law spectrum) and 1.22 (Raymond-Smith spectrum). Weaker limits are found if a broad iron edge is assumed: the 3 sigma upper limit of a 8.5 keV iron edge (1 keV smeared) is 3.1 (power law spectrum). For the Raymond-Smith spectrum no 3 sigma limit was found, only a 90% limit of 3.1.

3.4 ASCA Spectrum of Source 2

The observed spectrum for Source 2 from the S2 detector for P1, and the best fit Raymond-Smith model spectra is shown in Figure 4. Table 3 summarizes the results of fits for the S2 and S3 spectra for the two pointings for the three spectral models (power law, Raymond-Smith, and blackbody). The number of counts for Source 2 is significantly less than for LSI +61°303. Even so, the blackbody model has significantly worse χ_r^2 . The power law and blackbody spectra give very low column densities. This, together with the steep power law index, are a strong indication that the Raymond-Smith model is a better spectral model than a power law, and significantly better than blackbody.

The P1 and P2 spectra for Source 2 were consistent with having the same spectral parameters. Thus joint fits were carried out including P1 and P2 spectra. The power law and Raymond-Smith models both gave statistically acceptable fits. The last entry of Table 4 gives the resulting 90% limits on the spectral parameters. The Raymond-Smith spectral model is preferred here since the power law model gives a very low column density and very steep spectral index.

4 DISCUSSION

4.1 LSI +61°303

The ASCA instruments observed LSI +61°303 during 2 pointings at binary phases 0.2 and 0.43. Spectral fitting rules out the blackbody model, by the large χ_r^2 and the unrealistically low N_H derived from the fit. The Raymond-Smith hot plasma model is also unlikely: the fits have a higher χ_r^2 than the power law model; the derived plasma

temperature is very high; and more importantly, N_H is inconsistent with radio-derived value (Frail and Hjellming 1991). Thus the power law model is the only consistent model for the observed spectra.

The power law index is in the range 1.6 to 1.9, similar to that seen for classical X-ray pulsars. N_H is now well determined to be $5.5 - 6.5 \times 10^{21} \text{ cm}^{-2}$ (90% confidence), which is currently the best determination, and avoids the assumption on spin temperature needed for determination of column density from radio observations. The constancy of N_H for the two pointings shows there is no significant column density change with orbital phase, as might be expected if there was absorption in the wind of the Be star. The ASCA spectra show no evidence for Fe line emission and allow a strong upper limit to be placed on the intensity of any Fe line, and a weak limit to be placed on the presence of an Fe absorption edge. The lack of Fe line emission is important. All of the accreting X-ray pulsars for which good spectra have been obtained show Fe line emission. This is good evidence that the emission mechanism for LSI +61°303 is different than classical accreting X-ray pulsars. The low X-ray luminosity ($4.7 \times 10^{33} (\text{d}/2.3 \text{ kpc})^2 \text{ erg sec}^{-1}$) also argues against the classical accretion mechanism. The 2-10 keV flux is 30% lower in the second pointing. There is a difference in spectral index between the two pointings at the 90% confidence level, with P2 (phase 0.43) having the steeper spectrum (1.83 vs. 1.71) than P1 (phase 0.2).

In Figure 5, the X-ray and gamma-ray spectra of LSI +61°303 are summarized as a $\nu - F_\nu$ plot (for which equal luminosity per decade of frequency is a horizontal line). The P1 and P2 ASCA spectra, and the measurements reported from the MISO balloon (Perotti et al. 1980), Comptel (van Dijk et al. 1993), COS-B (Swanenburg et al. 1981), and EGRET (Thompson et al. 1995) experiments are shown. The MISO reported flux levels are more than an order of magnitude higher than the next highest points (those from Comptel), and are inconsistent with extrapolations from either the ASCA or Comptel spectra. Furthermore, the MISO points range in significance from 1 to 2 sigma and thus should be treated as upper limits.

The ASCA spectrum has been extrapolated to high energy for the different power law indices and normalizations (e.g. see Table 4). The best fit parameters for both ASCA pointings give spectra well below the Comptel measurements (see Fig. 5). Even the 90% upper limits are well below: i.e. the 90% upper limit to the flux at 10 MeV from the ASCA P1 spectrum is $0.043 \text{ keV/cm}^2 \text{ sec}$. However, the ASCA P1 spectrum does extrapolate to the COS-B and EGRET data: the 90% ASCA P1 upper and lower flux limits at 200 MeV are 0.026 and $0.131 \text{ keV/cm}^2 \text{ sec}$. The ASCA P2 spectrum 90% upper and lower flux limits at 200 MeV are 0.026 and $0.0049 \text{ keV/cm}^2 \text{ sec}$. The behaviour as a function of orbital phase or the long-term variability of the high-energy gamma-ray or of the X-ray

(2–10 keV) flux is not well measured for LSI +61°303, so the possible explanation of the above discrepancy is that the measurements sample different parts of the orbital period and different orbits. Since the Comptel and EGRET data sampled a large part (2 week viewing period) of the 26 day orbit it is more likely that the cause is orbit-to-orbit variability rather than different phase sampling at low and high energy. Without further observations, it cannot be concluded that the spectrum has an MeV bump.

The ASCA spectrum has also been extrapolated down in energy. Here we consider the overall spectrum of LSI +61°303 at times outside of radio outburst. The change of spectrum with binary phase is considered in the companion paper (Harrison et al. 1996), which discusses two frequency radio monitoring simultaneous with the X-ray observations. The radio spectrum of LSI +61°303 has been determined to be flat, although the spectral index is not well constrained (Gregory et al. 1979, Taylor and Gregory, 1984). A radio spectral index of 0.25 outside of radio outburst (equivalent to X-ray spectral index of 1.25) is found (Harrison et al. 1996) which is consistent with previous data. Using the mean spectral parameters for both the ASCA pointings, spectral index of 1.75 and power law normalization of 1.5×10^{-3} , the predicted flux density at 1.5 cm wavelength is 205 mJy. This is within the range of observed flux densities from LSI +61°303 during outburst, but the mean observed flux density outside outburst is near 20 mJy. In order to obtain 20 mJy at 1.5 cm, a break in spectral index from 1.75 to 1.25 is required near 200 GHz. The predicted flux density at the break frequency is 36 mJy.

4.2 Source 2

Source 2 has a spectrum which is likely thermal with temperature of 0.8 keV. This temperature is typical for the hot component for stellar coronal emission, for early type star stellar wind shock emission, for supernova remnants, or for emission from a spiral galaxy. The stellar interpretations are most likely, since a spiral galaxy would have a column density larger than LSI +61°303; and a supernova remnant would appear as an extended object (young compact supernova remnants would be hotter).

An attempt to identify Source 2 was made. Using the NED database, the search yielded no sources coincident with Source 2. It did yield three sources other than LSI +61°303 within the GIS fields of view: 4C +61.06, 87GB 023740.5+611333 and 87GB 023440.3+605537, and no other sources in the SIS fields of view. None of the three had any excess counts in S2 or S3, with 3 sigma upper limits to flux (2–10 keV) of 3×10^{-14} erg cm⁻² s⁻¹. A 10.9 photographic magnitude optical counterpart was found in the BD star catalog: BD 60536, classified as G2 (Brodskaia and Shajn 1958). This confirms that

Source 2 is very likely a stellar coronal source, it is unlikely to have affected any of the high energy measurements of LSI +61°303, which were made with instruments which could not resolve Source 2 from LSI +61°303.

4.3 X-ray Emission Models for LSI +61°303

Two models have been proposed to explain the radio outburst of LSI +61°303. Maraschi and Trevis (1981) postulate an interaction front between an OB star wind and the relativistic wind of a young pulsar. The relativistic electrons accelerated at the wind interaction shock front produce synchrotron radiation. The radio outbursts arise as a result of electrons radiating in a changing magnetic field at the interaction front due to an eccentric orbit. X-ray and gamma-ray emission is predicted from inverse Compton scattering of stellar photons on these same energetic electrons. Taylor and Gregory, 1984 propose a model in which a compact object in a highly eccentric orbit around an OB star accretes at supercritical rates via Roche Lobe mass transfer at periastron. The episodes of supercritical accretion produce energetic electrons which are observed in bursts of radio emission. Here also, inverse Compton scattering of stellar photons gives the X-ray and gamma-ray emission.

We now discuss how the ASCA observations shed new light on the emission mechanisms for LSI +61°303. Here we have shown, for the first time, that LSI +61°303 does in fact have a power law X-ray spectrum in the 0.5 to 10 keV energy range, and that it extrapolates up in frequency to match the gamma-ray spectrum at EGRET and COS-B energies. A spectral break is required to extrapolate the ASCA spectrum down in frequency to intersect the radio spectrum at 200 GHz. The power law radiation luminosity is dominated by higher energy photons: the radio luminosity (1.46 to 200 GHz) is 5.0×10^{28} erg/sec; the radio to X-ray (200 GHz to 1 keV) luminosity is 5.9×10^{33} erg/sec; the 1 to 10 keV luminosity is 4.7×10^{33} erg/sec; the 10 keV to 200 MeV luminosity is 1.2×10^{35} erg/sec. A distance of 2.3 kpc has been assumed here. The total non-thermal luminosity in all wavebands is about 1.3×10^{35} erg/sec. This is a serious problem for the supercritical accretion model, in which the expected luminosity is of order 10^{38} erg/sec.

The power law radiation energy density, using the above flux estimates, in the source region is 0.002 erg/cm^3 , for source size of 1.5 milliarcsec (Massi et al. 1993), compared to the magnetic field energy density of $0.003 (B/1 \text{ Gauss})^2 \text{ erg/cm}^3$. However the B0 companion star provides a larger radiation density (2 erg/cm^3 is the mean value inside a sphere of radius equal to the mean orbital separation for a B0 stellar luminosity of $1.3 \times 10^{38} \text{ erg/s}$), ensuring that inverse Compton losses dominate, unless the magnetic field,

B , is larger than about 26 Gauss and much higher than the equipartition value (with the relativistic electrons) of 1 Gauss (Massi et al. 1993). The ratio of inverse Compton losses on stellar photons to synchrotron losses is $(26/(B/1 \text{ Gauss}))^2$.

Independent of B , for a given electron energy spectral index, the inverse Compton and synchrotron spectra have the same spectral indices. However relativistic electrons of a given energy produce inverse Compton and synchrotron photons of different energies. Inverse Compton gamma-rays between 1 MeV and 200 MeV come from electrons emitting 460 (B/1 Gauss) GHz to 92 (B/1 Gauss) THz (0.38 (B/1 Gauss) eV) synchrotron photons. Inverse Compton X-rays from 1 to 10 keV come from the same electrons as 460 (B/1 Gauss) MHz to 4.6 (B/1 Gauss) GHz synchrotron photons. The inverse Compton spectrum has a lower cutoff at the stellar photon energy of a few eV, below which only synchrotron photons are emitted. The synchrotron spectrum has an upper cutoff or spectral break depending on the electron spectrum upper cutoff or break energy.

Consider the case of strong magnetic field ($B > 26$ Gauss). This is not ruled out by observations, since the synchrotron self-absorption frequency is 3.7 GHz for $B = 26$ Gauss, and is thus no inconsistent with radio measurements. If the electron spectrum extends to high energy then the full power law spectrum, radio through gamma-rays, could be due to synchrotron emission. Using a spherical source of angular size 1.5 milliarcsec (Massi et al. 1993, Taylor et al. 1992), and distance of 2.3 kpc (Gregory et al. 1979), the X-ray normalization gives the product of electron energy and (magnetic field) $^{((\gamma+1)/2)}$, where $\gamma=2.5$ is the power law index of the electron spectrum. For a magnetic field of 26 Gauss, the integrated electron energy between $2.4 - 7.6 \times 10^{11}$ eV (i.e. energy of electrons responsible for 1 to 10 keV photons) is 3.8×10^{34} erg. The total energy for electrons radiating above 200 GHz up to 200 MeV is 2.9×10^{36} erg. The main contribution is from the lower energy electrons. Electrons with energy less than 2.2×10^7 eV emit below 200 GHz. If there is a 200 GHz spectral break due to electron spectrum, the lower energy electrons have $\gamma=1.5$ and total energy (for 1.46 to 200 GHz photons) of 1.1×10^{33} erg. The other possibility is that the difference between the observed radio spectral index and the X-ray and gamma-ray spectral index is due to self-absorption in the radio band. Then $\gamma=2.5$ and the energy in low energy electrons is much larger: 7.0×10^{36} erg. The electron energy for X-ray to gamma-ray (i.e. above 10 keV) emitting electrons ($\gamma=2.5$) is 4.5×10^{34} erg. For larger B , the electron energies scale as $B^{-1.35}$.

However, the electron spectrum is unlikely to extend up to the value of $3.9 \times 10^{13} / \sqrt{B}$ eV necessary to give 100 MeV synchrotron photons. If we assume shock acceleration, confinement of the electrons in the acceleration region (size 1.5 milliarcsec) limits electron energy to less than $5.7 \times 10^7 B$ eV. Then the synchrotron spectrum can extend only up to 1.7×10^{-4}

B^3 eV or $41 B^3$ GHz. The higher energy non-thermal photons are due to inverse Compton emission, with an upper cutoff energy for the inverse Compton photons of $9.2 \times 10^4 B^2$ eV. This then restricts the minimum magnetic field to 33 Gauss to yield 100 MeV photons. The above discussion on electron energies is still valid for the low energy electrons. The high energy inverse Compton photons and radio synchrotron photons come from the same electrons, and there is no population of high energy electrons. The lack of an observed spectral break between 1 keV and 200 MeV for theThe absorbing column is constant between the two observations. inverse Compton radiation implies the emitted synchrotron spectrum doesn't have a break or cutoff between $4.6 (B/1 \text{ Gauss})$ MHz to $92 (B/1 \text{ Gauss})$ THz ($0.38 (B/1 \text{ Gauss})$ eV). In particular, the spectral break required between X-ray and radio should not be due to electron spectrum break but rather due to self-absorption. The intrinsic radio spectral index is 1.75, with the observed radio spectral index of 1.25 in the 1.4 to 5 GHz band caused by self-absorption. This is consistent since the predicted frequency where self-absorption sets in is the middle of the observed band of radio frequencies: $2(B/1 \text{ Gauss})^{0.2} \text{GHz}$, using the VLBI-measured angular size of LSI +61°303 (Massi et al. 1993).

The above discussion shows that the sub-eV (radio) spectrum should be synchrotron in origin, and the super-eV (X-ray to gamma-ray) spectrum should be inverse Compton in origin. The upper energy to the synchrotron spectrum is due the limits of the particle acceleration. In this case, from the known synchrotron and inverse Compton emissivities from a relativistic electron population, there is a single value of magnetic field which gives both the observed radio and X-ray fluxes. This value is 300 Gauss, and the resulting electron spectrum is of the form $3.0 \times 10^4 E^{-2.5} \text{cm}^{-3}$. Here we have assumed that the same population of electrons produces both the high energy and the radio emission. We have also taken the electron density and magnetic field to be uniform, so the values for both are average values in the emission region. In the case of low magnetic field ($B < 26 \text{ Gauss}$), the radio and X-ray emission come from two different populations of electrons. Additionally, the radio emitting electrons must be far from or shielded from the Be star to avoid strong inverse Compton losses. We do not consider such a complicated situation here.

In summary, the main features of the radio to gamma-ray spectrum of LSI +61°303 agree with an inverse Compton plus synchrotron model. The radiation above eV energies is inverse Compton in origin, that below eV energies is synchrotron. A high magnetic field of about 300 Gauss is required to give the observed radio and X-ray fluxes. The difference in spectral index in the observed radio band (1.25) and in the high energy bands (1.75) is due to self-absorption, which sets in at a frequency near 6 GHz. The X-ray and radio emission both originate in radiation from relativistic electrons, and therefore related to the mechanism for energetic particle production in LSI +61°303 . Discussion of what particle

production mechanism is appropriate to LSI +61°303 is dependent on what is known about the variation of both radio and X-ray emission with orbital phase. This is discussed together with the time-variability analysis of the ASCA data in (Harrison et al. 1996).

5 CONCLUSION

The ASCA observation of LSI +61°303 has provided a high quality spectrum for the first time. The spectrum is of power law form, with index 1.6-1.9, and the column density to LSI +61°303 is determined accurately as $5.5 - 6.5 \times 10^{21} \text{ cm}^{-2}$. There is evidence for spectral steepening by 0.12 in index between phase 0.2 and 0.43, coincident with a decrease in 2-10 keV X-ray flux by 30%. The upper limit on iron line emission indicates that LSI +61°303 is not a classical accreting X-ray pulsar.

We have examined the Comptel, COS-B and EGRET gamma-ray data. The ASCA power law spectrum extrapolates to high energy. It lies below the Comptel data points at a few MeV, but is in agreement with the COS-B and EGRET data near 200 MeV.

The X-ray to gamma-ray power law spectrum can be explained by an inverse Compton plus synchrotron model. Self-absorption results in an the observed radio spectral index different than the X-ray to gamma-ray index. If the relativistic electrons are shock accelerated, the magnetic field must be larger than 30 Gauss to produce the observed 100 MeV radiation. A magnetic field of about 300 Gauss is derived from matching the observed X-ray and radio fluxes to the inverse Compton plus synchrotron model.

DAL acknowledges support from the Natural Sciences and Engineering Research Council. FAH acknowledges support from a Robert A. Millikan Research Fellowship.

Table 1: Background Subtracted Countrates (ct/s)

Source	S0 Countrate	S1 Countrate	S2 Countrate	S3 Countrate
LSI P1	.1622 \pm .0034	.0797 \pm .0025	.1269 \pm .0035	.1253 \pm .0034
LSI P2	.0891 \pm .0023	.0648 \pm .0019	.0938 \pm .0023	.1115 \pm .0025
Source 2 P1	n/a	n/a	.0160 \pm .0015	.0128 \pm .0014
Source 2 P2	n/a	n/a	.0169 \pm .0011	.0166 \pm .0011

Table 2: Spectral Parameters for Spectra of LSI +61°303

Spectrum	Model	Param1 ¹	Param2 ¹	Param3 ¹	χ_r^2
S0, P1	power	.623-.830	1.62-1.88	$1.90-2.63 \times 10^{-3}$	0.91
	raym	.452-.558	11.0-20.7	$5.85-6.48 \times 10^{-3}$	1.06
	bbdy	.048-.154	.868-.952	.836-1.11	1.56
S1, P1	power	.613-.923	1.75-2.16	$1.32-2.15 \times 10^{-3}$	0.80
	raym	.450-.729	4.41-10.6	$3.57-4.44 \times 10^{-3}$	1.02
	bbdy	.026-.193	.784-.901	.615-1.02	1.19
S2, P1	power	.219-.536	1.39-1.73	$.950-1.49 \times 10^{-3}$	0.76
	raym	.112-.305	13.9-62.5	$3.96-5.01 \times 10^{-3}$	0.80
	bbdy	0-.019	.883-.987	.536-.766	1.36
S3, P1	power	.140-.472	1.32-1.64	$.875-1.38 \times 10^{-3}$	1.00
	raym	.061-.262	18.4-64.0	$4.13-5.33 \times 10^{-3}$	1.02
	bbdy	0-.020	.898-.992	.555-.761	1.45
S0, P2	power	.551-.753	1.78-2.07	$1.26-1.78 \times 10^{-3}$	0.89
	raym	.369-.511	5.97-11.1	$3.32-3.67 \times 10^{-3}$	1.11
	bbdy	.021-.132	.753-.831	.762-1.10	1.35
S1, P2	power	.440-.657	1.63-1.98	$.827-1.23 \times 10^{-3}$	1.02
	raym	.324-.454	7.21-13.4	$2.53-2.85 \times 10^{-3}$	1.09
	bbdy	0-.083	.764-.860	.523-.788	1.43
S2, P2	power	.199-.489	1.47-1.79	$.920-1.40 \times 10^{-3}$	0.72
	raym	.065-.226	12.4-37.8	$3.45-4.02 \times 10^{-3}$	0.78
	bbdy	0-.015	.826-.912	.623-.862	1.45
S3, P2	power	.381-.660	1.71-2.01	$1.28-1.89 \times 10^{-3}$	0.85
	raym	.133-.323	5.73-16.8	$3.43-3.85 \times 10^{-3}$	1.02
	bbdy	0-.017	.803-.873	.740-.978	1.42

¹90% confidence range given; see text for description of parameters

Table 3: Spectral Parameters for Spectra of Source 2

Spectrum	Model	Param1 ¹	Param2 ¹	Param3 ¹	χ_r^2
S2, P1	power	0-.216	3.41-5.09	$3.58-7.74 \times 10^{-4}$	0.62
	raym	.144-.666	.454-.879	$.391-1.73 \times 10^{-3}$	0.53
	bbdy	0-.209	.156-.221	35.5-472	1.00
S3, P1	power	0-.286	3.32-5.19	$3.60-9.13 \times 10^{-4}$	1.07
	raym	.138-.865	.374-.928	$.839-3.78 \times 10^{-3}$	0.81
	bbdy	0-.119	.181-.296	7.96-124	1.38
S2, P2	power	0-.085	2.78-3.54	$2.09-3.11 \times 10^{-4}$	0.66
	raym	.148-.810	.572-1.08	$.581-1.04 \times 10^{-3}$	0.80
	bbdy	0-.064	.231-.306	4.54-19.6	1.23
S3, P2	power	0-.098	2.44-3.17	$2.38-3.70 \times 10^{-4}$	0.52
	raym	0-.068	1.27-2.24	$3.83-5.17 \times 10^{-4}$	0.56
	bbdy	0-.073	.234-.355	2.97-19.3	1.01

¹90% confidence range given; see text for description of parameters

REFERENCES

- Bignami, G., et al., 1981, *ApJ*, 247, L85
- Brodskaya, E.S., and Shajn, P.F., 1958, *Izv. Krymsk. Ap. Obs.*, 20, 299
- Frail, D. and Hjellming, R. 1991, *AJ*, 101, 2126
- Gregory, P. and Taylor, A. 1978, *Nature*, 272, 704
- Gregory, P. et al. 1979, *AJ*, 84, 1030
- Harrison, F., Leahy, D. and Waltman, E. 1996, *ApJ*, submitted
- Hutchings, J. and Crampton, D. 1981, *PASP*, 93, 486
- Maraschi, L. and Treves, A. 1981, *MNRAS*, 194, 1p
- Massi, M., Paredes, J., Estalella, R. and Felli, M. 1993, *A&A*, 269, 249
- Perotti, F. et al. 1980, *ApJ*, 239, L49
- Swanenburg, B. et al. 1981, *ApJ*, 243, L69
- Tanaka, Y., Inoue, H. and Holt, S. 1994, *PASJ*, 46, L37
- Taylor, A. and Gregory, P. 1984, *ApJ*, 283, 273
- Taylor, A. Kenny, H., Spencer, R. and Tzioumis, A. 1992, *ApJ*, 395, 268
- Thompson, D. et al. 1995, *ApJSuppl.*, 101, 259
- van Dijk, R., Bloemen, H., Hermesen, W., et al. in *Proceedings of the Second Compton Symposium*, AIP conf. proc. 304, p324, 1993
- von Montigny C, *et al.*, (EGRET Collaboration), *IAU Circ.* no. 5708, Feb. 13, 1993

Table 4: Spectral Parameters for Joint Fits to Spectra

Model	Param1 ¹	Param2 ¹	Param3 ¹	Flux(2-10) ²	Flux(0.5-2) ²	χ_r^2
LSI, P1						
S0+S1+S2+S3						
power	.544-.670	1.63-1.78	1.43-1.74x10 ⁻³	6.05x10 ⁻¹²	1.17x10 ⁻¹²	1.31
raym	.369-.439	13.1-21.0	4.47-4.80x10 ⁻³	6.64x10 ⁻¹²	1.15x10 ⁻¹²	1.44
bbdy	0-.034	.911-.960	.615-.734	4.35x10 ⁻¹²	1.11x10 ⁻¹²	1.81
LSI, P2						
S0+S1+S2+S3						
power	.532-.645	1.75-1.90	1.21-1.45x10 ⁻³	4.25x10 ⁻¹²	9.67x10 ⁻¹³	1.20
raym	.355-.428	8.18-11.3	3.29-3.47x10 ⁻³	4.65x10 ⁻¹²	9.48x10 ⁻¹³	1.32
bbdy	0-.029	.829-.869	.638-.752	2.88x10 ⁻¹²	9.41x10 ⁻¹³	1.73
Source 2						
P1+P2,S1+S2						
power	0-.036	3.02-3.46	2.74-3.36x10 ⁻⁴	1.43x10 ⁻¹³	7.53x10 ⁻¹³	1.05
raym	.398-.673	.666-.872	5.11-8.61x10 ⁻⁴	6.65x10 ⁻¹⁴	4.13x10 ⁻¹³	1.12
bbdy	0-.025	.230-.273	9.58-24.0	2.55x10 ⁻¹⁴	4.94x10 ⁻¹³	1.62

¹90% confidence range given; see text for description of parameters

²2-10 keV or 0.5-2 keV flux in erg cm⁻² s⁻¹ given for the best fit model spectrum

FIGURE CAPTIONS

FIGURE 1: ASCA S2 contour map of the LSI +61°303 field.

FIGURE 2: ASCA S0 spectrum of LSI +61°303 , first pointing, with power law model spectrum.

FIGURE 3: ASCA S2 spectrum of LSI +61°303 , first pointing, with power law model spectrum.

FIGURE 4: ASCA S2 spectrum of Source 2, first pointing, with Raymond- Smith model spectrum.

FIGURE 5: Summary of high energy measurements of LSI +61°303 .

Figure 5

